PROCEEDINGS, 43rd Workshop on Geothermal Reservoir Engineering
Stanford University, Stanford, California, February 12-14, 2018
SGP-TR-213

Numerical Strategy for Uncertainty Quantification in Low Enthalpy Geothermal Projects

Sannidi Shetty, Denis Voskov, David Bruhn

Stevinweg 1, 2628 CN Delft

d.v.voskov@tudelft.nl

Keywords: low enthalpy geothermal, uncertainty quantification, thermal breakthrough.

ABSTRACT

One of the most important technological characteristics in low enthalpy geothermal projects is the time when cold fluid from the injection well breaks into the production well. In this study, we identified a large sensitivity of thermal breakthrough time to the position of the well doublet in a hot sedimentary aquifer with the fixed geological scenario. These variations can greatly impact the lifetime of the low enthalpy geothermal project, thereby affecting the project's economy. Here we investigate the main factors responsible for the variation of breakthrough time by performing a sensitivity analysis of different hydraulic, thermal and numerical parameters. The geological modeling software Flumy was used to generate detailed fluvial facies distributed similarly to that observed in the West Netherlands Basin (Nieuwerkerk Formation). The models were then populated with various thermal and hydraulic properties, correlated with the facies map. Various scenarios were run in ADGPRS (Automatic-Differentiation General Purpose Research Simulator) to perform a sensitivity analysis. For given technological characteristics (distance between doublet wells, injection and production rates, drainage area etc.), a difference of approximately 50% was observed in the lifetime of the project by changing the doublet positions and keeping the same distance between the doublet pair. The major numerical and geological factors contributing to the difference in breakthrough time were identified and ranked in this study. In addition, the best simulation strategy and numerical parameters for uncertainty quantification in low enthalpy geothermal projects are suggested.

1. INTRODUCTION

The West Netherlands Basin (WNB) is a 60-km-wide basin in the southwest of the Netherlands (Donselaar et al., 2015). WNB stands as an example for a promising aquifer region in the Netherlands (Vondrak, 2016). Sandstone-rich fluvial successions of the Nieuwerkerk Formation are the main targets for heat exploitation in the WNB. WNB also accounts for 70% of all deep geothermal doublets currently in operation in the Netherlands. The fluvial Delft Sandstone Member (DSSM), part of the Lower Cretaceous Nieuwerkerk Formation (Willems, 2017, Wiggers, 2009) is also the main target for the Delft Aardwarmte Project (DAP). In recent years, geothermal technology has received substantial attention as an alternative source of energy. However, the lack of detailed information about subsurface formations of interest often introduces significant uncertainties to the technological and economic planning of geothermal projects. As the result, some important technological parameters, affecting geothermal projects, cannot be predicted with enough certainty.

One of the major uncertainties in a geothermal project is the lifetime of the reservoir. The lifetime of geothermal projects with doublets installed parallel or perpendicular to the paleoflow direction of the fluivial sandstone system of the WNB and corresponding pump energy losses have been studied by Willems et al. (2017). It was observed that the lifetime of the aquifer was shorter when the doublets were placed perpendicular to the paleoflow. A lifetime of the reservoir can be sensitive to numerous factors. Several studies investigating factors influencing heat flow in geothermal reservoirs and their lifetime have been carried out. These include viscosity and density dependence on temperature (Zheng et al., 2010, Watanabe et al., 2010, Saeid and Hicks, 2015), porosity and permeability (Mottaghy et al., 2010, Ekneligoda and Min, 2014, Vogt et al., 2013), geothermal fluid salinity (Saeid et al., 2013), flow rate (Franco and Vaccaro, 2014), well spacing (Sauty et al., 1980), injection temperature (Bedre and Anderson, 2010) and reservoir geometry (Sippel et al., 2013). But these factors have not been tested on the influence of the spread between breakthrough curves obtained by changing the location of the doublets.

In order to obtain breakthrough curves, the very first requirement is the regional geological model that describes the spatial distribution of a fluvial system. Delft Sandstone Member (DSSM) in the Lower Cretaceous Nieuwerkerk Formation, present in the West Netherlands Basin (WNB), has been used as a case study. To obtain the breakthrough curves, an ensemble of models were created using Flumy. Flumy helps to replicate the depositional heterogeneity which is the result of the sand-body continuity combined with the permeability trends within the sand body. These models were then populated with reservoir parameters using a beta distribution. In order to perform numerical simulations and modeling of geothermal reservoirs, ADGPRS (Automatic-Differentiation General Purpose Research Simulator) was used (Voskov and Tchelepi, 2012; Wong et al. 2015).

To reduce uncertainties in parameter estimation, a sensitivity study of various parameters (such as porosity, permeability, heat conduction, heat capacity) was performed on the generated models. In addition, the effect of over and under burden layers and the thickness of the reservoir were looked upon. They were then followed by identifying the well performance and investigation of flow paths using streamlines. Finally, the influence of temporal and spatial resolution was looked upon.

In our work, we observed that the lifetime of the reservoir varied significantly just by relocating the doublets from their original position to their neighboring positions tens of meters away. A difference of 25-35 years was observed when the position of doublets was changed. We identified main physical mechanisms and parameters affecting this spread. These parameters were ranked by the

importance for a given geological scenario. In addition, the influence of numerical parameters (such as timestep size and grid resolution) were estimated and the optimal set of parameters was proposed.

2. MATHEMATICAL FORMULATION

2.1 Governing Equations

The governing equations of fluid flow represent mathematical statements of the conservation laws of physics.

Mass conservation equation: The standard mass conservation equation of a system having n_c components and n_p phases can be represented as:

$$\underbrace{\frac{\partial}{\partial t}\left[\phi \sum_{c/p=1}^{n_{c/P}} x_{cp}\rho_p S_p\right]}_{Accumulation} + \underbrace{\nabla.\left[\sum_{p=1}^{n_p} x_{cp}\rho_p u_p\right]}_{flux} + \underbrace{Q_M}_{\substack{Source/Sink \\ flux}} = 0 \tag{1}$$

where ϕ is the porosity of the rock, $\rho_p$is the mass density of phase p, S_p is the saturation of phase p, $u_p$is the Darcy/superficial velocity of phase p, $Q_M$is the source/sink term for mass conservation equation. The subscripts c/p refers to the components and phases respectively.

In our study, single phase compressible pure water was considered. Hence the eq. (1) reduces to:

$$\frac{\partial}{\partial t}[\phi\rho_w] + \nabla.[\rho_w u_w] + Q_M = 0 \tag{2}$$

Momentum balance: Darcy's law was used for momentum balance equation. It is used to express fluid velocity in terms of pressure gradient:

$$u_p = -\underbrace{\frac{KK_{rp}}{\mu_p}}_{mobility\ term}\underbrace{\left[\nabla p_p + \rho_p g \nabla z\right]}_{potential\ term} \tag{3}$$

where u_p is the superficial velocity of phase p, K is the rock permeability, K_{rp} is the relative permeability for phase p, μ_p is the viscosity of phase p, p_p is the pressure of phase p, ρ_p is the mass density for phase p, g is the gravitational constant, z is the downward depth along the vertical. Please note that the negative sign comes from the potential term.

In our model, the eq. (3) is reduced to

$$\mathrm{u} = -\frac{\mathrm{K}}{\mu}[\nabla \mathrm{p} + \rho_{\mathrm{w}} \mathrm{g} \nabla \mathrm{z}] \tag{4}$$

Combining the two eq. (2) and (4) we have:

$$\frac{\partial}{\partial t}[\phi\rho] - \nabla.\left[\frac{\rho K}{\mu}[\nabla p + \rho g \nabla z]\right] + Q_M = 0 \tag{5}$$

The objective of the simulator (ADGPRS) is to compute pressures for each grid cell, such that the conservation of mass is fulfilled at any time. Please note that the equation is highly nonlinear since quantities like density and viscosity are functions of pressure and temperature (Sebastian 2016).

Energy Conservation Equation: For the heat transport, the transfer in porous matrix is governed by both conduction and convection and can be expressed as follows:

$$\underbrace{\frac{\partial}{\partial t}\left[(1-\phi)\rho_r U_r + \phi \sum_{c/p=1}^{n_{c/P}} \rho_p U_p S_p\right]}_{Accumulation} + \underbrace{\nabla.\left[\sum_{c/p=1}^{n_{c/p}} H_p \rho_p u_p\right]}_{\substack{heat\ transport \\ with\ fluid\ flux \\ (convection)}} + \underbrace{\nabla.(\kappa \nabla T)}_{\substack{heat\ flux \\ (conduction)}} + \underbrace{Q_E}_{\substack{Source/Sink \\ flux}} = 0 \tag{6}$$

where ϕ is the porosity of the rock, $\rho_r$is the mass density of rock, U_r is the internal energy of the rock, $\rho_p$is the mass density of phase p, U_r is the internal energy of phase p, S_p is the saturation of phase p, $u_p$is the Darcy/superficial velocity of phase p, H_p is the phase enthalpy of phase, Q_E is the source/sink term in energy conservation equation. The subscripts r refers to rock and f refers to fluid. In our model, the eq. (6) is reduced to

$$\frac{\partial}{\partial t}[(1-\phi)\rho_r U_r + \phi\rho_w U_w] + \nabla.[H_w\rho_w u_w + (\kappa\nabla T)] + Q_E = 0 \quad (7)$$

The objective of the simulator (ADGPRS) is to compute temperature for each grid cell, such that the conservation of energy is fulfilled at any time. Please note that the equation is also nonlinear since quantities like internal energy and enthalpy are functions of pressure and temperature. (Sebastian 2016). A detailed description of discretized equations, construction of residual and Jacobian matrix can be found in (Voskov and Tchelepi,2012; Wong et al., 2015).

2.2 Streamlines

The concept of streamlines is used for a long time in reservoir engineering (e.g. Muskat and Wycoff's, 1934). It has received repeated attention to numerically predict the movement of fluid. In cell-based simulation techniques like finite difference or finite elements, the phase saturation and components are transported from cell to cell, whereas the streamline simulations follow a flow based grid technique along which the transport of fluid occurs (Thiele et al., 2002). Streamline is a path traced by a massless particle moving with the flows which are tangential to the velocity of the moving fluid. It is generally used in conventional reservoir simulation to visualize the flow field that defines the capture zones of the well. It can also be used to estimate sweep efficiency, check accuracy in upscaling techniques, evaluate the efficiency of injectors and producers. To compute streamlines in our study, the nonlinear solution of coupled conservation for mass and energy is solved first. Once the pressures are obtained at the nodes of the grid cell, we compute velocity at every interface of all the grid cells using Darcy's law. A more detailed description of streamlines can be obtained in (Crane and Blunt, 1999; Thiele et al., 2002).

3. MODELLING

3.1 Geometric and Property Modeling

The very first goal of this work was to create a geological model that describes the facies distribution which could then be used for flow simulations. The modeling technique is similar to the one used by Willems (2017), which is based on the subsurface dataset of the fluvial Nieuwerkerk Formation of the WNB. The top of Delft Sandstone member (DSSM), one of the stratigraphic units with known reservoir properties, is present at a depth of 2000-2300m. Bottom-hole temperature readings from oil and gas wells in the region indicate that the geothermal gradient is approximately 3°C/100m (Donselaar et al., 2015). In the current well doublets, 65-75˚C formation water is produced and re-injected at 30-40˚C. The doublets are placed 1-2 km apart to obtain a lifetime of at least 30 years and to prevent the risk of having an early cold water breakthrough (Donselaar et al., 2015). With an aim to maintain pressure support in the reservoir, the doublets target the same reservoir. Therefore, it is essential to have an understanding of the reservoir connectivity between the production and the injection wells in the reservoir. The flow rates in these doublets are in the range of 100-200 m^3/hr (Willems, 2017).

On the basis of studies on rock cores from old oil and gas wells, five different facies were recognized namely floodplain fines, crevasse splays, single-story channel bodies and amalgamated sandstone complexes (Willems, 2017). The point bar grows through lateral accretion and is characterized by a fining upward sequence. Based on the maximum fining upward sequence, an estimate on the height of each channel deposition could be made. This was then related to the maximum height of the other channels. Using this information, the thickness (depth) of individual sandstone bodies was observed to be approximately 4m. Based on the bank flow depth, the bank flow width was estimated at 40m. Crevasse splay thickness in the cores ranged from 0.2-0.6m. The gamma rays provided a range of net to gross ranging from 15% to 85%. In addition, using the petrophysical data of a single well, a permeability-porosity relationship was obtained (Willems et al., 2017) as follows:

$$\boldsymbol{K = 0.0633\, e^{(29.507\,\phi)}} \quad (8)$$

Although the DSSM has highly faulted structures, the model does not include faults, in order to reduce the complexity of the problem. Geological modeling of a fluvial reservoir is intricate as it comprises heterogeneity in sediment bodies. Fluvial reservoirs primarily comprise impermeable floodplains and permeable sandstone bodies (Willems, 2017). In order to obtain a realistic geological model similar to the DSSM, the geometry-based modeling software Flumy was used. As it mirrors sedimentary processes this technique produces numerical blocks that are geologically realistic (Lopez et al., 2012).

The ensemble of models having varying net-to-gross (N/G) were created. An increase in the net-to-gross ratio (N/G) helps in increasing the amount of sand bodies(reservoir units) in the model. Various fluvial deposits, such as point bars, crevasse splays, overbank alluvium, sand and mud plug are generated in the model as seen in Figure 1. Their distributions were simplified into two categories, reservoir, and non-reservoir units. Facies such as crevasse splays, overbank deposits, levees and mud plugs were considered as non-reservoir grid blocks and are identified as shale bodies. While the reservoir grid blocks consisted of point bars, sand plugs, and channel lags. These are identified as sandstone bodies.

The visualization of this simplified model can be found in Figure 2. The shale bodies were assumed to be impermeable and homogenous with a permeability of 5mD and porosity of 10% (Willems et al., 2017). For the reservoir units (sandstone bodies), a beta distribution correlation function was used to generate a heterogeneous porosity field based on the WNB core plug porosity measurements (Willems et al., 2017). The beta distribution characteristics include mean, standard deviation, skew and kurtosis of 0.28, 0.075, 0.35 and 2.3 respectively (Willems et al., 2017). Once the porosities were distributed, the permeability was assigned to each grid using the permeability-porosity relationship from equation (**8**). Thermal properties such as heat conduction and heat capacity were considered to be homogeneous and isotropic within each facies. Specific values of heat capacity and conductivity were chosen for sands and shales

respectively. Densities and thermal properties have been chosen among typical values for sedimentary deposits and are based on references (Eppelbaum et al., 2014; Willems et al., 2015; Saeid et al., 2015; Saeid and Hicks, 2015).

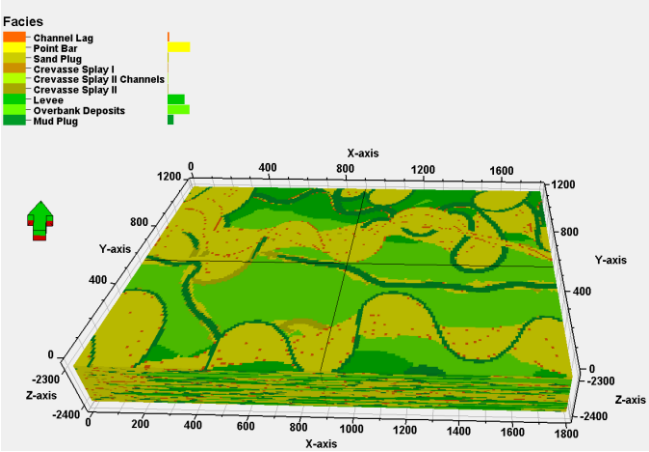

Figure 1: Visualization of fine scale model (180x120x40 grids) having N/G of 35% (with all facies deposits)

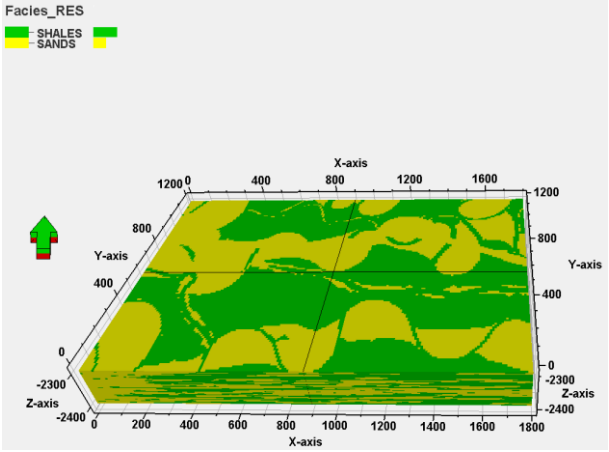

Figure 2: Visualization of fine scale model (180x120x40 grids) having N/G of 35% (with facies reduced to sands and shale deposits)

Since our model has an initial temperature of 75˚C and an initial pressure of 200 bar, the formation fluid exists in the liquid phase. Hence our model ignores the presence of gas (steam) and all the simulations were done assuming single phase single component water.

3.2 Inclusion of Over and Under Burden

Once the reservoir model was populated with thermal and fluid properties, an over and under burden layer was modeled above and below the reservoir respectively as shown in Figure 3. These layers were assumed to be a single thick block of 400m thickness each. A finer vertical discretization only resulted in a slight delay in the breakthrough while the trend in the thermal breakthrough to the production well remained the same. These layers were distributed with homogenous thermal and fluid properties. The porosity and permeability of these layers were set to a lower value of 5% and 0.1mD respectively. This was done to confine the fluid flow within the reservoir.

SANDSTONES				**SHALES**			**OVER AND UNDER BURDEN LAYERS**		
Parameter	**Symbol**	**Value**	**Unit**	**Symbol**	**Value**	**Unit**	**Symbol**	**Value**	**Unit**
Permeability range	K	6-3000	mD	K	5	mD	K	0.1	mD
Porosity range	ϕ	15-38	%	ϕ	10	%	ϕ	5	%
Specific heat capacity	C	730	J/Kg-K	C	950	J/Kg-K	C	950	J/Kg-K
Volumetric heat capacity	cp	1934.5	KJ/m^3-K	cp	2470	KJ/m^3-K	cp	2470	KJ/m^3-K
Thermal conductivity	κ	2.65	W/m-K	κ	2	W/m-K	κ	2	W/m-K
Volumetric thermal conductivity	κ	229	KJ/m-day-K	κ	172.8	KJ/m-day-K	κ	172.8	KJ/m-day-K
Density	ρ	2650	Kg/m^3	ρ	2600	Kg/m^3	ρ	2600	Kg/m^3

Table 1: Overall properties distributed to the reservoir model

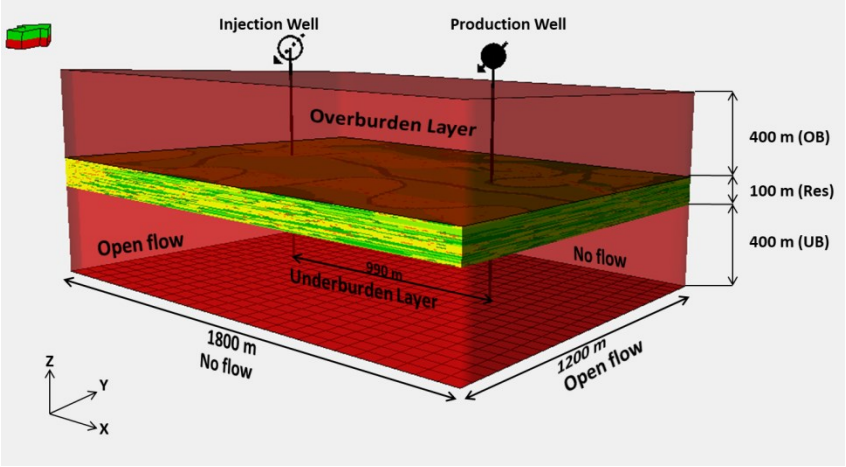

Figure 3: Inclusion of over and under burden impermeable layer to the reservoir model and representation of boundary conditions

Parameter	Symbol	Value	Unit
Reservoir depth	Z	2300	m
Overall thickness of the reservoir	the	100	m
Reservoir Vertical discretization	layers	40	nos.
Thickness of overburden layer	thk_{OB}	400	m
Thickness of under burden layer	thk_{UB}	400	m
Reservoir lifetime temperature	$T_{lifetime}$	340	K
Initial reservoir pressure	p_i	200	Bars
Borehole diameter	d	0.2	m
Water injection and production rate	q_{inj}, q_{prod}	4800	m^3/day
N/G variation range	N/G	15-75	%
Distance between doublet pair	$\Delta_{doublet}$	990	m

Table 2: Generalized properties used in the models

3.3 Well Placements and Well Identification

Once the model was populated with all the parameters during the dynamic and property modeling, the next step was to place injector and producer wells. The two wells were spaced 990m apart and are perforated through all the 40 layers of the reservoir. The alignment of the wells was designed to be perpendicular to the channel planes, and the wells are located at the center of the model. Since large variations were observed in the thermal breakthrough with changing well locations, eight neighboring coordinates surrounding the center (indicated green in Figure 4) were selected as well locations for performed simulations. Note that during every simulation, a single pair of wells was chosen. More importantly, only the location of the doublet was changed during the simulation, while the distance between the doublets always remained the same as seen in Figure 6A and B. In Figure 6, plots C and D indicate the breakthrough curve of A and B respectively. In Figure 6E both the doublets (as seen in 6A and 6B) are re-represented to indicate that the location of the doublet was just shifted by a single grid. Figure 6F shows the comparison of the thermal breakthrough curves when the wells were placed in the Centre and Southeast. We can observe a decrease in the lifetime of the reservoir by 30 years when the doublet is relocated from the Centre to the Southeast. This difference in the lifetime of the reservoir is termed as the spread in the breakthrough.

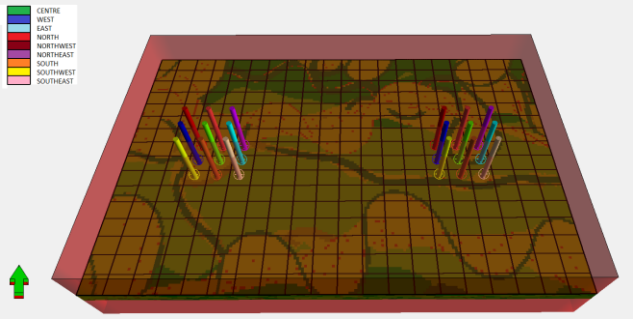

Figure 4: placement of wells with the center identified as green and the other doublets located at the neighboring grid cells in a fine scale model with NG35%.

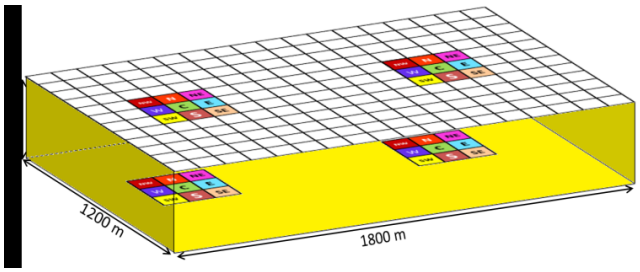

Figure 5: Illustrates the locations at which the doublet was placed. A difference of 30 years was observed in the lifetime of the reservoir when the doublets was relocated from the west to the north in a coarse model having 60 x 40 x 40 grids

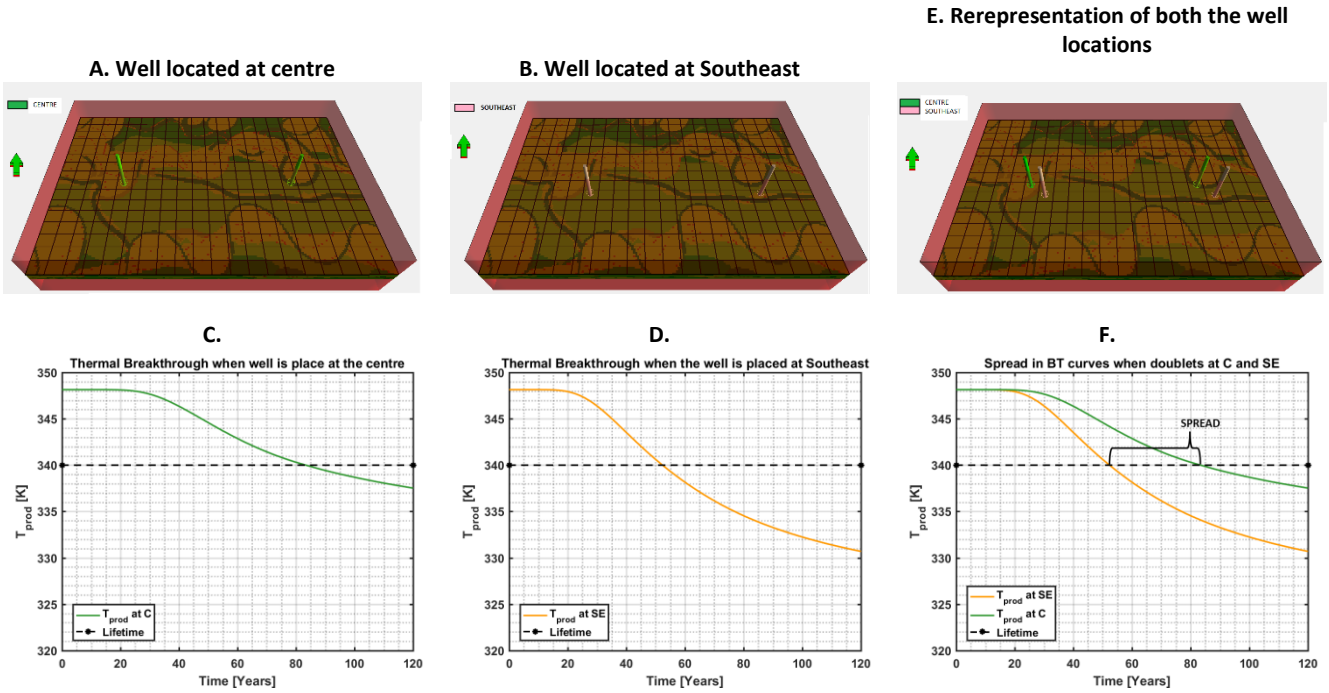

Figure 6: Images A and B represent the visualization of the doublet located at the center and southeast respectively. Plots C and D indicate the corresponding breakthrough curve of A and B respectively at injection and production rates of 4800m3/day. Image E indicates the position of the doublets and the plot F describes the spread in the breakthrough curves just by relocating the doublet.

4. RESULTS

The workflow implemented in this study is similar to the approach used by Willems et al. (2017). The only difference was the software, used for simulation. In our study, we used ADGPRS, which is based on a finite-volume discretization, while Willems et al. (2017) used COMSOL, which is based on a finite element approach. The validation of the conventional geothermal formulation in the ADGRPS framework was performed in Wong et al. (2015) and Khait and Voskov (2016).

4.1 Base Case Model

In order to obtain a base case model, an ensemble of geological models was generated using Flumy. The range of parameters used for generating static geological models is described in section 3.1 and 3.2. Using these ranges in input parameters, several coarse scale models with wide channel deposits were generated with N/G (net to gross) ranging between 15%-75%. These models were populated with hydraulic and thermal properties as described in section 3.1 for both the reservoir and the under and overburden layers and then simulated using the ADGPRS simulator. Amongst the wide range of models, N/G 35% was observed to have a significant difference in

the lifetime of the reservoir when the doublets were placed at different locations. According to Willems et al. (2017), this value of N/G is quite typical for the reservoir in the study. Figure 7 represents the variation in the breakthrough curves when the model (N/G 35%) was simulated for doublets moved around to different locations. From Figure 8, it can be observed that the system has a lifetime of 34 years when the well was placed in the West and a lifetime of 62 years when the well was relocated to the North. Since the aim of the thesis was to investigate the root cause of this spread/variation in the lifetime, these two extreme cases were chosen for the sensitivity study.

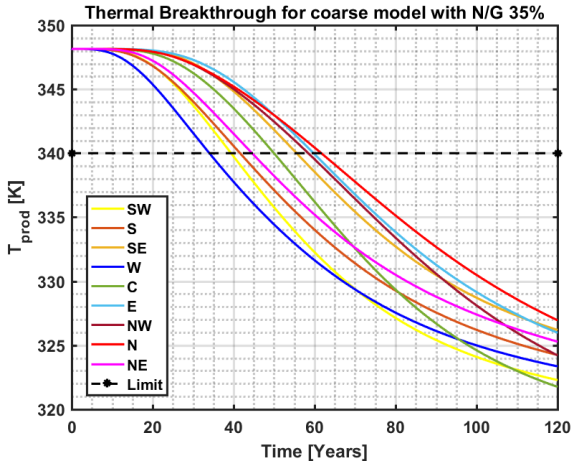

Figure 7: BT curves for all the nine coordinates(center(C), west(W), east(E), northwest(NW), north(N), northeast(NE), south(S), southwest (SW) and southeast (SE)) for a coarse model with N/G 35%

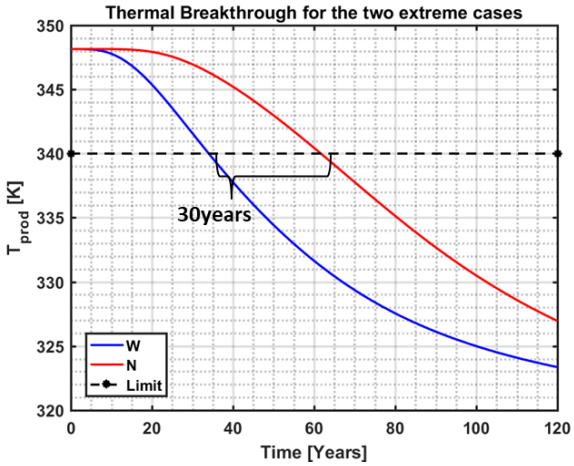

Figure 8: BT curves for the two doublet locations (west (W) and north (N)) that showed a significant difference of 30 years in the reservoir lifetime.

4.2 Sensitivity Analysis on Base Case Model

4.2.1 Thermal Rock Heat Conductivity

Heat transfer in a geothermal system mostly occurs by convection and, to a lesser extent, by conduction. This is because most of the flow simulations are generally representative of a braided system where the flow is generally straight and has minimum hindrance from the rock. However, since we deal with the meandering systems, there is a lot more interaction between the fluids and rocks and hence thermal conductivity also plays a role.

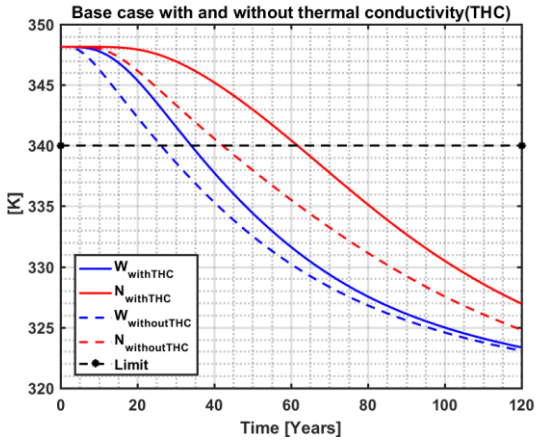

Figure 9: Variation in the BT trajectories from the base case while ignoring the heat conductivity of the rock.

Parameter	Base Case Model	Model ignoring Rock Heat Conductivity
	Rock Heat Conductivity [κ] (KJ/m-day-K)	
Sandstone	228.96	0
Shale	172.8	0
Water	57.88	57.88
	Spread (Years)	
	28	16

Table 3: Comparison of the base case with the simulation results from ignoring rock heat conductivity

In Figure 9, the solid lines represent the base case model which includes the presence of rock heat conductivity while the dotted curves indicate the breakthrough curves when the heat conductivity is completely ignored. In our base case simulations, the cold water, which is injected into the reservoir, is contacting the surrounding porous volume with higher temperature. The heat is transferred from the higher to the lower temperature region thereby increasing the temperature in the cold water. Over time, as the injected cold water propagates through the reservoir, it is heated up by the rock matrix. Hence the cold waterfront is not moving with the injected water, thereby resulting in a delay in the breakthrough time compared to the travel time of the water.

On ignoring the rock conductivity, there is no conductive recharge taking place between grid blocks with the cold water and its neighboring grid blocks. Hence, due to the absence of this heat flux, an early breakthrough would result. However, our main aim was to identify if this parameter significantly contributes to a change in the spread of the breakthrough curves between the North and West location. It was observed that it does not really play a significant role.

4.2.2 Rock Heat Capacity

In Figure 10**,** the solid lines (base case) represent the breakthrough curves when the rocks have a specific heat capacity of approximately 2000 kJ/m^3-K, while the dotted lines represent the breakthrough curves when the rock's specific heat capacity is completely ignored. The higher the specific heat, the longer is the ability of the rock to retain heat. Since in the base case rocks can retain heat for a greater duration, there is a greater thermal recharge of water which thereby delays the thermal breakthrough of the cold waterfront. From the graph in Figure 10, it can be observed that the rock heat capacity can play a significant role in the variation of the breakthrough curves.

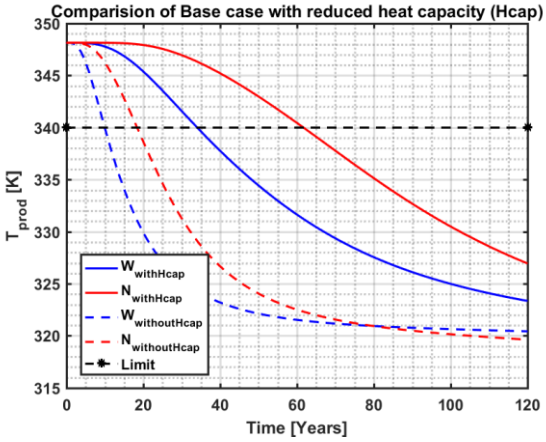

Figure 10: Variation in the BT trajectories from the base case while ignoring the heat capacity of the rock.

Parameter	Base Case Model	Model ignoring Rock Heat Capacity
	Rock Heat Capacity [cp] (KJ/m^3-K)	
Sandstone	1934.5	0
Shale	2470	0
Water	4187	4187
	Spread (Years)	
	28	9

Table 4: Comparison of the base case with the simulation results from ignoring rock heat capacity

It can be noticed that the rock heat capacity does play quite an important role in the thermal breakthrough curves. This is because the introduction of rock heat capacity in the model creates two fronts within the reservoir. One is the thermal front, which is the front at which we observe a temperature difference and the other is the injected waterfront. On ignoring the rock heat capacity in the model, both of these fronts travel together, while, in the presence of rock heat capacity, we can observe a delay in the thermal front compared to injected waterfront due to the additional recharge from the rocks. A plot of the two front propagations in a simple homogeneous 1D setup with the rock heat capacity is shown in Figure 11.

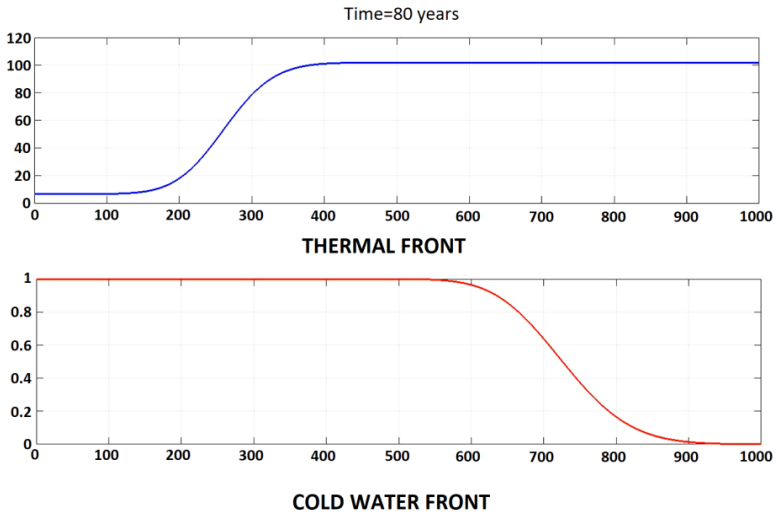

Figure 11: Front propagations during the presence of the rock heat capacity

4.2.3 Elimination of Local Heterogeneity

Even when heat capacity differences are taken into account, a significant difference in the spread is still observed and hence we also tested the influence of several other factors, mainly the effect of heterogeneity in the sandstone bodies. In the base model, sandstone bodies were highly heterogeneous. This heterogeneity is now eliminated and a model with constant permeability for sands (1600mD) and another constant permeability value for shale (5mD) was generated.

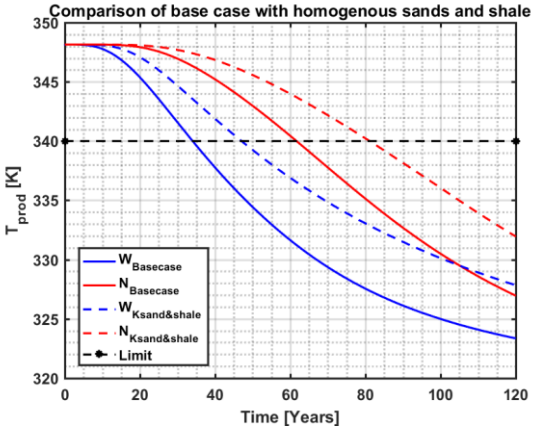

Figure 12: Variation in the BT trajectories from the base case while constant permeabilities were assigned for sands and shale.

Parameter	Base Case Model	Model eliminating local heterogeneity
	Permeability [K] (mD)	
Sandstone	6-3500	1600
Shale	5	5
	Spread (Years)	
	28	34

Table 5: Comparison of base case with the simulation results from assigning constant permeability for sands and shales

The results in Figure 12 show that the heterogeneity of the sand bodies does not cause the large variations in the breakthrough time. However, the resulting breakthrough times are entirely different which also suggest that in the heterogeneous model, the fluid travels a completely different flow path from the homogeneous model. The easiest way to strengthen the argument that the spread in the breakthrough plots could likely be because of change in the flow path is to run the simulation for a completely homogenous model.

4.2.4 Eliminating Global Heterogeneity

A fully homogenous model was considered, where both the sands and shales were assigned a constant permeability of 1600mD. In a fully homogenous model, the flow path would behave the same irrespective of the location of the well. Hence there would be no change in breakthrough time what so ever (see Figure 13). Therefore, the result obtained from a fully homogenous model bolsters the fact that the spread in the breakthrough curves is largely dependent on the geological formations which control flow path of the fluid.

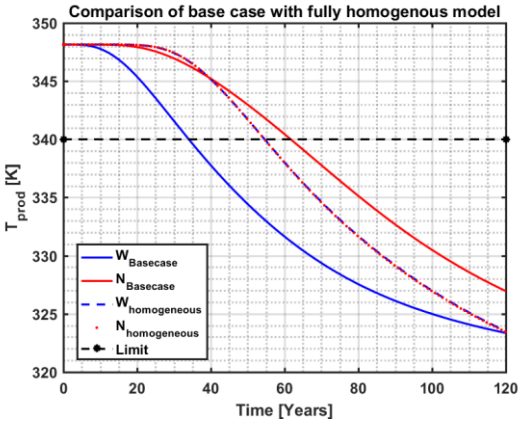

Figure 13: Variation in the BT trajectories from the base case with the fully homogenous model.

Parameter	Base Case Model	Model eliminating global heterogeneity
	Permeability [K] (mD)	
Sandstone	6-3500	1600
Shale	5	1600
	Spread (Years)	
	28	0

Table 6: Comparison of base case with the simulation results of a fully homogenous model

On the basis of the above findings, we can argue that a detailed analysis of the flow paths need to be performed to understand the concept of connectivity and thermal recharge.

4.3 Well Performances

From the above calculations, we derive the possible reason for the spread in the breakthrough, the variation in the flow path from each injection location. However, a closer look into the flow path of the fluids is required to explain this phenomenon. In order to do so, we analyzed the well performances at each well location. For this purpose, injection and production rates for each of the 40 layers accessed by the wells were calculated.

The well performance at the two well locations (N and W) of the base case was examined. The well performances were nearly identical at every time step since water is low compressible and we deal with pseudo-steady state conditions.

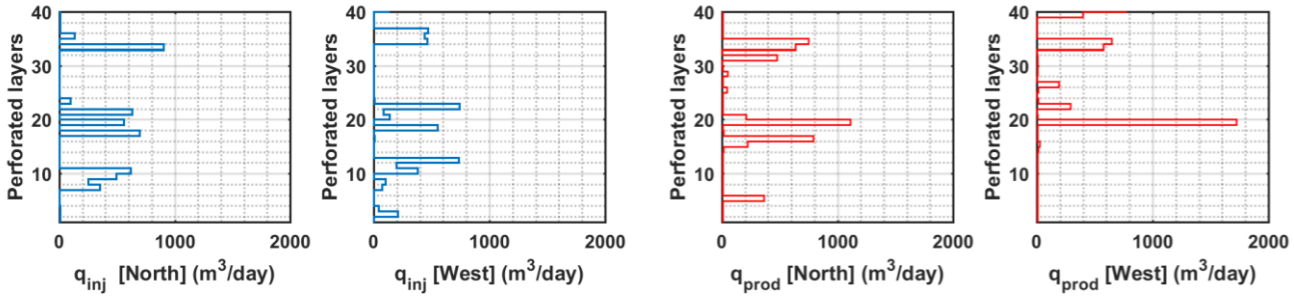

Figure 14: Well performances indicating the variation in the (left) injection rates and (right) production rates between well at north and west

Figure 14 presents the comparison of the injection and production rates of the doublet located in the north versus rates of the doublet located in the east. The results show that the injection and production rates for the various layers were vastly different for the two well locations (W and N). A possible explanation for this could be that the injection rates along each perforated layer depend on the permeability of the perforated location. A highly permeable location would allow greater injection and production rates. In order to get a better insight, a comparison between the well performances and the associated permeability for each well was performed.

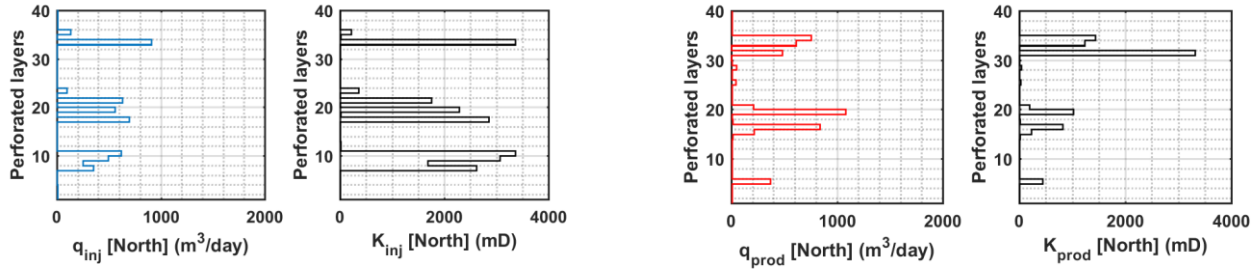

Figure 15: Illustration of (left) injection rates q_{inj} and (right) production rates q_{prod} with their associated permeability's

The relationship between the injection and production rates with the associated permeabilities (Figure 15) reveals a similar trend. However, there is no direct correlation between rate and permeability of the perforation. This indicates that just by relocating the doublets to the neighboring grid, the respective injection and production rates can be completely different due to the variations in the well connectivity to the fluvial channels. Such variations imply the possibility of various preferred flow paths between the injection and production wells. The various flow paths can be visualized with the help of streamlines.

4.4 Visualization with Streamlines

Streamlines are used to give us an intuitive understanding of the flow path. This, in turn, allows us to visualize the drainage regions associated with doublet wells. Streamlines tend to connect paths that are tangential to the high velocities vectors in the model. A high velocity is mostly observed in locations with high permeability and greater injection rates. From the performances of both the injection wells (N and W), streamlines were generated and plotted, starting in the layers with the large injection rates. Each streamline was assumed to be representative of injection volume of 200m^3/day.

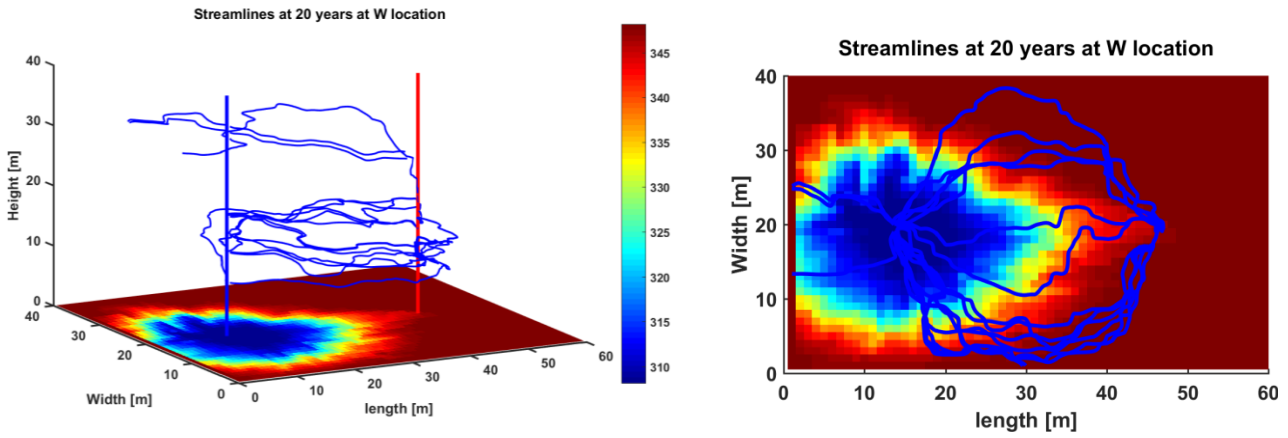

Figure 16: Illustration of the flow path from the layers with high injection rates at location W, at the base is the thermal front of the layer (22) that had the maximum injection rate.

From the streamlines in Figure 16 and Figure 17**,** it is clear that the layers having maximum injection rates for the two well locations (W and N) differ vastly. Just by relocating the wells a few meters away from the original location, the wells communicate with the reservoir through completely different layers resulting in a different flow path. In Figure 16 and Figure 17, a top view of the streamlines was plotted at both well locations. The base of the streamline plots represents the thermal front of the layer that had the maximum injection rates. After 20 years of simulation time, the propagation of the cold front is greater when the wells were located in the west. This difference in the propagation of the cold front is due to the different lengths of the flow paths in the N and W locations. Therefore we can expect an earlier breakthrough from the wells located in the west, compared to those in the North. From this observation, we can conclude that it's not only the connectivity of the injection and production wells that play a vital role but also the connectivity within the reservoir that contributes significantly to the variation in lifetime.

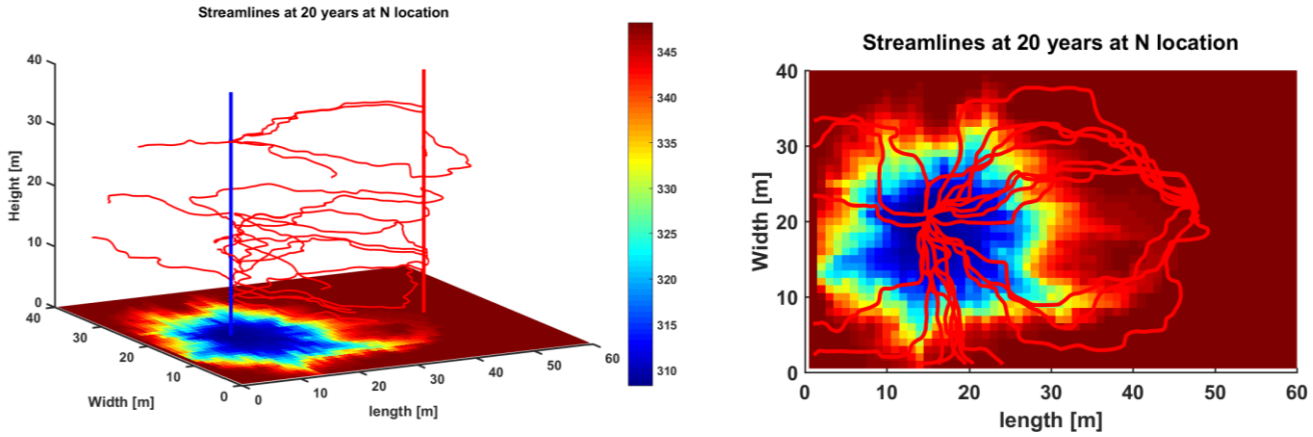

Figure 17: Illustration of the flow path from the layers having high injection rates at north location, at the base is the thermal front of the layer 33 that had the maximum injection rate.

4.5 Concept of Thermal Recharge

The concept of thermal recharge can be better explained with the help of synthetic 2D models. In the first model, a single fluvial channel between two doublets is introduced. In the second model, two channels connect the wells, see Figure 18 for illustration.

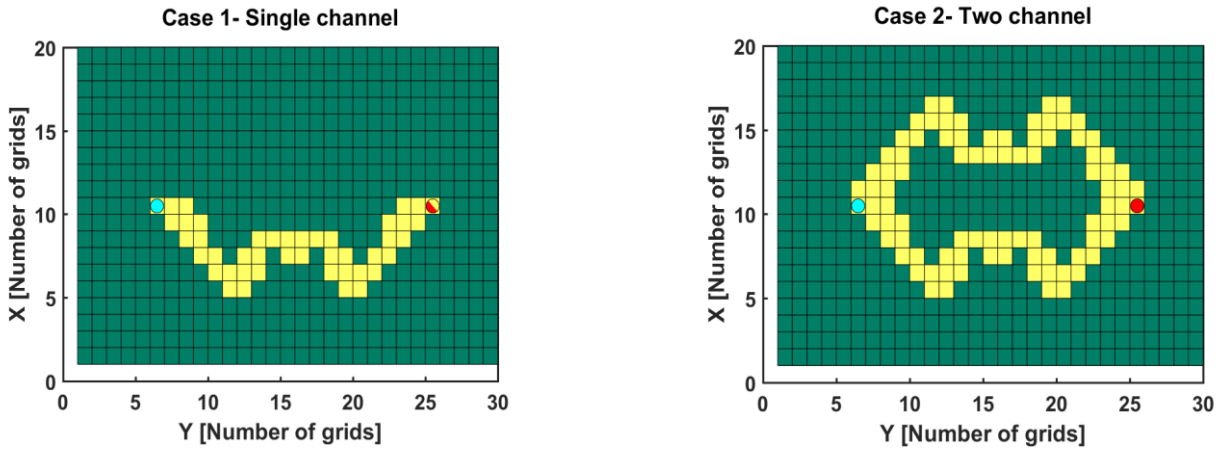

Figure 18: Illustration of the 2D model with (left) well encountering a single channel, (right) well encountering two channels.

All the thermal and fluid properties used in the model were kept the same for both the models and the injection and production rates were also maintained at a constant rate of $5m^3$/day for both cases. By running the simulation of both models for 120 years, the thermal breakthrough curves were obtained (Figure 20). It can be observed that case 1 has an earlier breakthrough compared to case 2. In case 1, since the flow is across a single channel, there is more volume of fluid flowing through it compared to case 2, wherein the volume of the fluid is split between two channels. Hence in case two, the fluids travel at a lower velocity and have more contact time with the rock matrix. This allows the fluids to recharge more effectively compared to case 1. This, therefore, results in a delay in the breakthrough of the cold-water plume as observed in Figure 19.

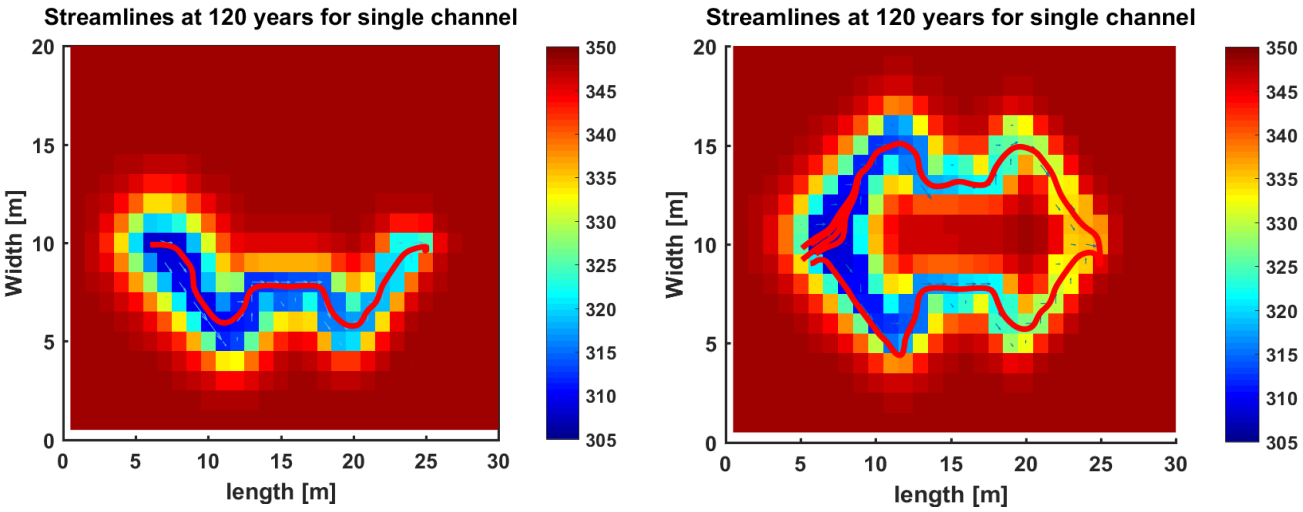

Figure 19: Streamline plots for the two cases (left) with a single channel and (right) with two channels. The color bar indicates the temperature of the waterfront in the reservoir

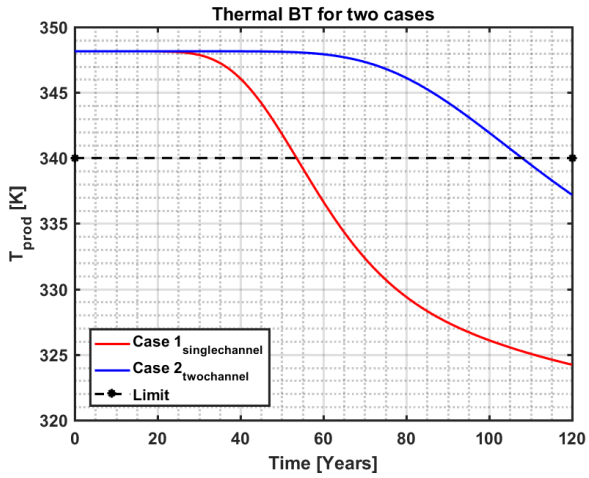

Figure 20: Thermal breakthrough comparison for Case 1 and Case 2

4.6 Tornado Plot

Along with the above-mentioned sensitivity analysis several other parameters were tested. These include:

i. **Reducing the variogram range of porosity and permeability:** The porosities were observed to range from 16% to 37% with almost 40% of the sand bodies having porosity values above 35%. In nature, these ranges of porosities represent loosely consolidated sands and are very unlikely to be observed in a reservoir that is 2.3km deep. Hence the porosities in our calculations were reduced to values ranging from 11% to 28%. Due to the empirical relationship between porosity and permeability, the range of permeability is also significantly reduced. Applying these changes to the base case, the model was simulated again. The results were almost analogous to the initial base case model with only subtle variations in the breakthrough time.

ii. **Reducing the thickness of the model by 50%:** The base case simulations were performed on a reservoir with a thickness of 100m discretized into 40 layers. Here, an attempt was made to identify the sensitivity in the thickness of the reservoir. In this analysis, all the 40 layers of the model were taken into consideration, however, the vertical size of each layer was now considered 1.25m apart, while in the base case every layer was 2.5m apart, resulting in a reduced reservoir thickness of 50m, which is half of what it was used in the base case (100m). To account for the reduced volume, the injection rates were also reduced to half. Despite reducing the thickness of the reservoir, there was still a significant spread of the breakthrough curves. Hence, it could be inferred that the thickness of the reservoir also does not play a major role to explain these huge spreads.

iii. **Ignoring over and under burden:** analysis of the effect of over and under burden layers was performed. The overburden and under burden layers were assumed to be impermeable zones and only contributed to thermal conduction. Comparing the plots of the base case and the model without over and under burden layers, no great effect on the spread was observed.

The relative influence of all the parameters discussed here on the variation of a thermal breakthrough is compared in a tornado plot in Figure 21.

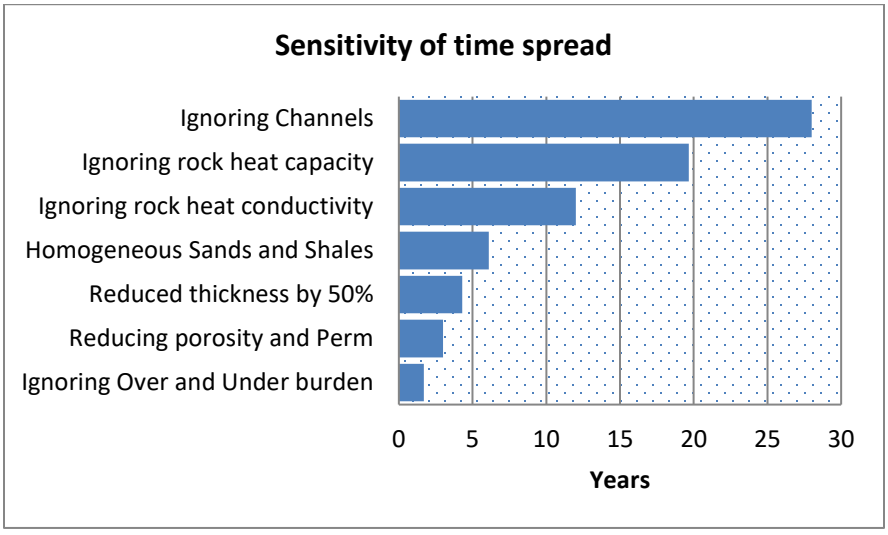

Figure 21: Tornado plot showing the influence of various parameters in the variation of thermal breakthrough

4.7 Temporal and Spatial Resolutions

The results, reported in the sensitivity study can also be affected by various numerical parameters of the simulations. The most important parameters are the resolution of temporal and spatial scale. For example, if the grid resolution is too coarse, the continuity of fluvial channels may be interrupted by numerical artifacts (such as grid blocks become disconnected). In addition, large time step can introduce large time truncation errors which can affect the physical solution as well. Hence it was required to check that our numerical results are not affected by errors in numerical approximation.

To identify if time step could affect the results, reported above, the base model with wells located in the North was run with varying time steps starting from 61,122 and 365 days. The results were the same irrespective of the time step used (see Figure 22 for reults). Hence it is evident that the time step is not affecting variations in thermal breakthrough. In addition, no time step cuts were detected in all simulation scenarios which indicates a similar time-truncation error.

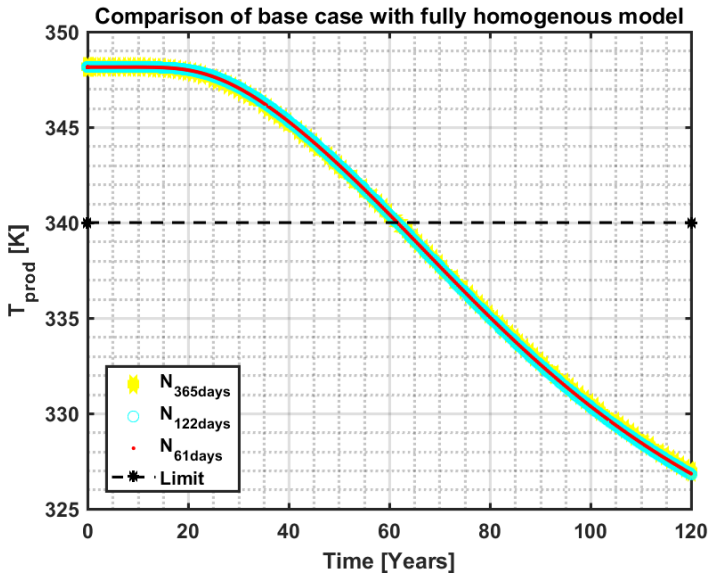

Figure 22: Base model ran with different time steps

The next aim is to identify if the spatial resolution of the model can influence the variation. Here we generate a fluvial model at a finer resolution and upscaled it to the resolution used above. The idea behind this procedure is to analyze the breakthrough variations between the fine and coarse grid models using the same geological structure. The fine scale model was upscaled in two ways as shown in Figure 23. The porosity was upscaled using volumetric averaging for both the types. For permeability, geometric upscaling was used for type 1 and a combination of arithmetic and harmonic upscaling was used for type 2.

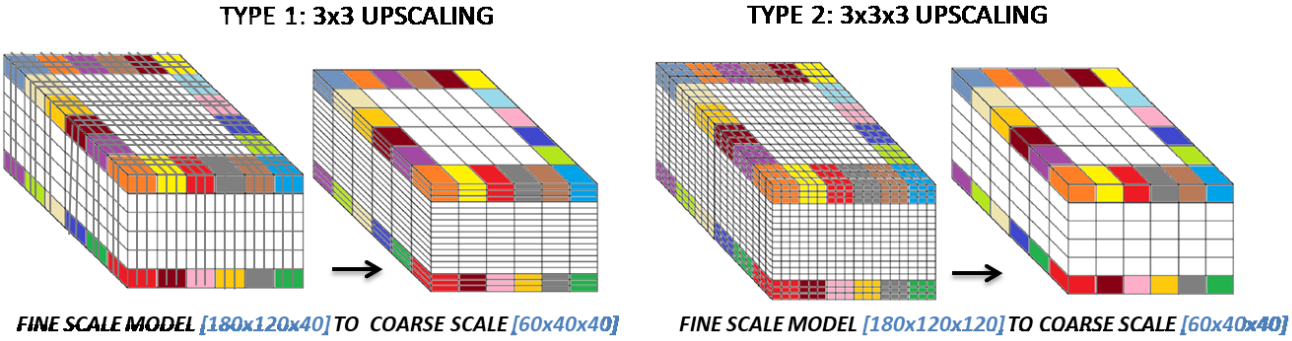

Figure 23: Base model upscaled in two ways (type 1 and type 2)

For both the upscaling types, the results were similar to the fine scale results (Figure 24). An upscaling procedure only introduced a loss in fine-scale details of sand bodies but preserved the geological architecture in which the channels were deposited. Thus, the spread in the breakthrough times for different well locations was still observed in the upscaled model.

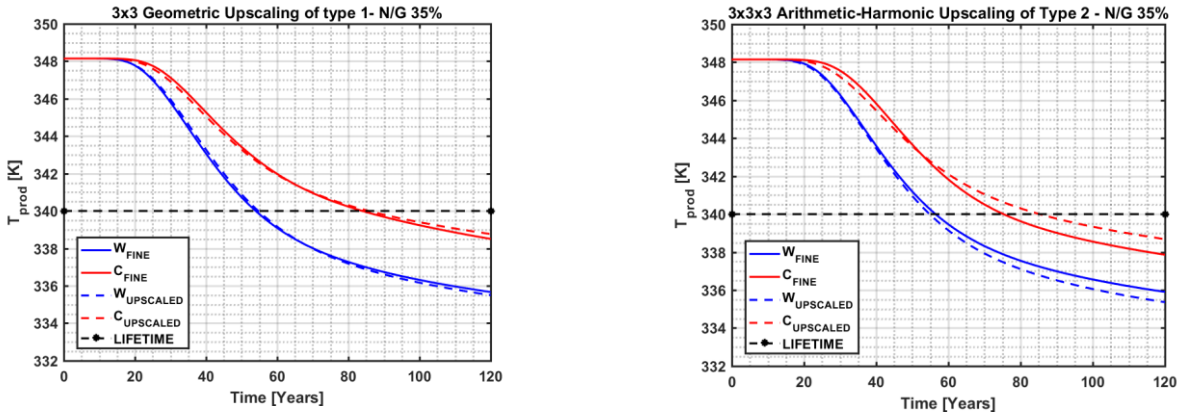

Figure 24: Left figure shows the upscaled results were quite accurate using the geometric upscaling technique for a 3x3 model. Right figure shows the upscaled results for Arithmetic-Harmonic averaging of a 3x3x3 model.

5. CONCLUSION

The main target of this study was to investigate the reasons for a large variation in the breakthrough time at different well locations of a well doublet in a low-enthalpy geothermal project. Scrutinizing the well performances, along with the produced streamlines from each doublet location and looking into the cross-sections of the generated model, it was evident that the cause of these large variations in thermal breakthrough was because of the large-scale geological heterogeneity (deposition of fluvial channels). It was observed that just by relocating the well to its nearest position, the injected cold water encounters an entirely different pathway. This resulted in a completely new fluvial path distribution compared to the fluvial path at the original doublet location. The variation in flow paths, in turn, affects the way in which the cold water is thermally recharged along the reservoir, resulting in a completely different breakthrough time when compared to that of its neighboring doublet locations. We demonstrate that the difference in the breakthrough time is also affected by other physical parameters and rank them by the strength of influence. Based on the sensitivity analysis, the rock heat capacity was found to have the largest influence on the thermal breakthrough time. Consequentially, thermal conductivity and fine-scale heterogeneity affect the variation in thermal breakthrough to a lesser extent. This ranking can help to identify the influential parameters whose accurate evaluation can reduce uncertainties in the performance prediction of low-enthalpy projects in similar geological formations. Comparing the fine- and coarse-scale models with the same N/G showed no significant influence on the calculated variations. This means that, despite having a better connectivity along the sand bodies in fine scale models, the variations were still evident which validate the accuracy of the numerical model.

REFERENCES

Bedre, M.G. and Anderson, B.J. "Sensitivity analysis of low-temperature geothermal reservoirs: effect of reservoir parameters on the direct use of geothermal energy: Geothermal Resources Council Transactions." Geothermal Resources Council 2012 annual meeting, 2010.

Willems, C.J.L.,.Nick, H.M., Donselaar, M.E., Weltje, G.J., Bruhn, D.F. "On the connectivity anisotropy in fluvial Hot Sedimentary Aquifers and its influence on geothermal doublet performance." (Geothermics) 65 (2017).

Chen, Y., Durlofsky, L.J., Gerritsen, M. and Wen, X.H. "A coupled local-global upscaling approach for simulating flow in highly heterogeneous formations." (Advances in water resource) 2003.

Crane, M.J. and Blunt, M.J. "Streamline-based simulation of solute transport." (WATER RESOURCES RESEARCH,) 35 (1999).

Donselaar, M.E., Groenenberg, R. and Gilding, D.T. "Reservoir Geology and Geothermal Potential of the Delft Sandstone Member in the West." Melbourne, Australia: World Geothermal Congress 2015, 2015.

Ekneligoda, T.C. and Min, K.B. "Determination of optimum parameters of doublet system in a horizontally fractured geothermal reservoir." (Renewable Energy ,152-160) 65 (2014).

Eppelbaum, L., Kutasov, I. and Pilchin, A. *Applied Geothermics.* Springer Science & Business, 2014.

Franco, A. and Vaccaro,M. "Numerical simulation of geothermal reservoirs for the sustainable design of energy plants: A review." (Renewable and Sustainable Energy Reviews 987–1002) 30 (2014).

Khait, M. and Voskov, D. "Operator-based Linearization for Modeling of Low-enthalpy Geothermal Processes." Stanford, California: Workshop on Geothermal Reservoir Engineering, 2016.

Lopez, Hamm, V., and Simon. "IMPACT OF FLUVIAL SEDIMENTARY HETEROGENEITIES ON HEAT TRANSFER AT A GEOTHERMAL DOUBLET SCALE." Stanford, California: Thirty-Seventh Workshop on Geothermal Reservoir Engineering, 2012.

Donselaar, M. E. Remco M. Groenenberg, Douglas T. Gilding. "Reservoir Geology and Geothermal Potential of the Delft Sandstone Member in the West." Melbourne, Australia: World Geothermal Congress 2015, 2015.

Khait, M. and Voskov, D. "Operator-based Linearization for Modeling of Low-enthalpy Geothermal Processes." Stanford, California: Workshop on Geothermal Reservoir Engineering, 2016.

Mottaghy, D., Pechniga, R. and Vogt, C. "The geothermal project Den Haag: 3D numerical models for temperature prediction and reservoir simulation." (Geothermics 40(3) 199–210) 2010.

Muskat, M. and Wyckoff. "A Theoretical Analysis of Waterflooding Networks." (Society of Petroleum Engineers) 107, no. 01 (1934).

Saeid, S. and Hicks, M. "Experimental and Numerical Study of Heat Flow under Low-Enthalpy Hydrothermal Conditions." 2015.

Saeid, S. Hicks, M. . "Experimental and Numerical Study of Heat Flow under Low-Enthalpy Hydrothermal Conditions." 2015.

Saeid, S., Khoury, R.A. and Barends, F. "An efficient computational model for deep low-enthalpy geothermal systems." (Computers & Geosciences, 400–409) 51 (2013).

Saeid, S., Khoury, R.A., Nick, H.M. and Hicks, M.A. "A prototype design model for deep low-enthalpy hydrothermal systems." (Renewable Energy) 77 (2015).

Sauty, J.P., Gringarten, A.C., Landel, P.A. and Menjoz, A. "Lifetime optimization of low enthalpy geothermal doublets." (Advances in European geothermal research, Springer, Netherlands , pp. 706-719) 1980.

Sebastian, Gries. "System-AMG Approaches for Industrial Fully and Adaptive Implicit Oil Reservoir Simulations." 2016.

Sippel, J., Fuchs, S., Cacace, M., Braatz, A., Kastner, O., Huenges, E. and Wenderoth, M.S. "Deep 3D thermal modelling for the city of Berlin (Germany)." (Environ Earth Sci, 70 , pp. 3545-3566) 8 (2013).

Thiele, M.R., Batycky, R.P. and Thomas, L.K. "Miscible WAG Simulations using streamlines." (European conference on the mathematics of oil recovery) 2002.

Vogt, C., Strahser, K.I., Marquart, G., Arnold, J., Mottaghy, D., Pechnig, R., Gnjezda, D., Clauser, C. "Modeling contribution to risk assessment of thermal production power for geothermal reservoirs." (Renewable Energy, 230-241) 53 (2013).

Vondrak, A.G. *(Bio-) stratigraphic correlation of geothermal aquifers in the West Netherlands Basin.* Panterra Geoconsultants, 2016.

Voskov, D. V., and Tchelepi, H. A.: Comparison of nonlinear formulations for two-phase multi-component EoS based simulation. *Journal of Petroleum Science and Engineering*, 82, 101-111 (2012).

Voskov, D. and Zhou, Y. "AD-GPRS Stanford University's Automatic Differentiation based General Purpose Research Simulator user manual, website: http://pangea.stanford.edu/researchgroups/supri-b/." n.d.

Watanabe, N., Wang, W., McDermott, C.I., Taniguchi, T. and Kolditz, O. "Uncertainty analysis of thermo-hydro-mechanical coupled processes in heterogeneous porous media." (Comput Mech, 45:263–280) 2010.

Wiggers, C.J.I. "The Delft Sandstone in the West Netherlands Basin." Delft, 2009.

Willems, C.J.L. *Doublet deployment strategies for geothermal Hot Sedimentary Aquifer exploitation.* Ph.D Thesis, 2017.

Willems, C.J.L., Goense, T., Nick, H.M. and Bruhn, D.F. "The relation between well spacing and Net Present Value in fluvial Hot Sedimentary Aquifer geothermal doublets; a West Netherlands Basin case study." Stanford, California: 41st Workshop on Geothermal Reservoir Engineering, 2016.

Willems, C.J.L., Nick, H.M., Donselaar, M.E., Weltje, G.J. and Bruhn, D.F. "On the connectivity anisotropy in fluvial Hot Sedimentary Aquifers and its influence on geothermal doublet performance." (Geothermics) 65 (2017).

Willems, C.J.L., Nick, H.M., Weltje, G.J., Donselaar, M.E. and Bruhn,D.F. "Influence of fluvial sandstone architecture on geothermal energy production." Melbourne, Australia: World Geothermal Congress, 2015.

Wong, Z.Y., Horne, R. and Voskov, D. "A Geothermal Reservoir Simulator with AD-GPRS." Melbourne, Australia: Proceedings World Geothermal Congress 2015, 2015.

Zheng, Ma, R. and Chunmiao. "Effects of Density and Viscosity in Modeling Heat as a Groundwater Tracer." (Ground Water;48(3):380-9) 2010.